A flux tower site attribute dataset intended for land surface modeling

Jiahao Shi[1], Hua Yuan[1], Wanyi Lin[1], Wenzong Dong[1], Hongbin Liang[1], Zhuo Liu[1], Jianxin Zeng[1], Haolin Zhang[1], Nan Wei[1], Zhongwang Wei[1], Shupeng Zhang[1], Shaofeng Liu[1], Xingjie Lu[1], Yongjiu Dai[1]

5   [1]Southern Marine Science and Engineering Guangdong Laboratory (Zhuhai), Guangdong Province Key Laboratory for Climate Change and Natural Disaster Studies, School of Atmospheric Sciences, Sun Yat-Sen University, Zhuhai 519082, China

Correspondence to: Hua Yuan (yuanh25@mail.sysu.edu.cn)

10   **Abstract.** Land surface models (LSMs) should have reliable forcing, validation, and surface attribute data as the foundation for effective model development and improvement. Eddy covariance flux tower data are considered the benchmarking data for LSMs. However, currently available flux tower datasets often require multiple aspects of processing to ensure data quality before application to LSMs. More importantly, these datasets lack site-observed attribute data, limiting their use as benchmarking data. Here, we conducted a comprehensive quality screening of the existing reprocessed flux tower dataset,

15   including the proportion of gap-filled data, external disturbances, and energy balance closure (EBC), leading to 90 high-quality sites. For these sites, we collected vegetation, soil, topography information, and wind speed measurement height from literature, regional networks, and Biological, Ancillary, Disturbance, and Metadata (BADM) files. Then we obtained the final flux tower attribute dataset by global data product complement and plant functional types (PFTs) classification. This dataset is provided in NetCDF format complete with necessary descriptions and reference sources. Model simulations

20   revealed substantial disparities in output between the attribute data observed at the site and the defaults of the model, underscoring the critical role of site-observed attribute data and increasing the emphasis on flux tower attribute data in the LSM community. The dataset addresses the lack of site attribute data to some extent, reduces uncertainty in LSMs data source, and aids in diagnosing parameter as well as process deficiencies. The dataset is available at https://doi.org/10.5281/zenodo.10939725 (Shi et al., 2024).

1 Introduction

Land surface models (LSMs) simulate the exchange of carbon, water and energy fluxes between soil, vegetation and atmosphere, and are essential tools for comprehending and predicting mass and energy interactions between the earth's biosphere and atmosphere (Pitman, 2003; Williams et al., 2009). The key role of LSMs is to provide the land surface boundary conditions for climate and weather forecast models (Mariotti et al., 2018; Pitman, 2003), as well as uncoupled

30   stand-alone runs to investigate terrestrial water resources, ecology, and carbon storage (Crow et al., 2012; Humphrey et al.,

2021; Ukkola et al., 2016a). Therefore, LSMs offer valuable insights for addressing environmental issues and mitigating climate change. Offline (i.e., uncoupled) LSMs are forced by meteorological data including wind speed, air temperature, specific humidity, air pressure, precipitation, and downward longwave and shortwave radiation. Flux towers measure the cycling of carbon, water and energy between the biosphere and atmosphere, providing observations with meteorological data that can be used to force offline LSMs. These observations are characterized by high temporal resolution (typically 30 min), continuous observations, measure fluxes directly, and often over multiple years. For these, they are regarded as benchmarking data for LSMs calibration, evaluation, and enhancement, allowing the development of models from sub-daily to seasonal and interannual scales. Numerous studies have leveraged flux tower data for developing LSMs (Best et al., 2015; Blyth et al., 2010; Harper et al., 2021; Melton et al., 2020; Stevens et al., 2020; Ukkola et al., 2016b; Zhang et al., 2017; Stockli et al., 2008). However, despite their significance, flux tower data was not originally designed for LSMs. When applied to LSMs, it suffers from poor data quality and a deficiency of attribute data.

FLUXNET2015 is currently the most widely used flux tower dataset (Pastorello et al., 2020), but substantial preprocessing is frequently required to ensure the reliability of meteorological forcing and flux assessment data for LSM applications. To reduce the repetitious data processing efforts and improve consistency, Ukkola et al. (2022) integrated three flux tower datasets (FLUXNET2015, La Thuile, and OzFlux), then performed screening, gap-filling, and other procedures to resolve issues such as missing data and energy balance closure (EBC) within these datasets. As a result, a dataset called PLUMBER2 with a total of 170 high-quality sites is tailored for LSMs. This work considered as many available flux tower datasets as possible and used an automated, reproducible data screening process. It's worth noting, though, that the dataset only performs quality checks on meteorological forcing and not on flux assessment data, to obtain more available years and enable models to be assessed against specific weather and climate events. Consequently, a large proportion of gap-filled flux data is present in some sites. Land surface modelers usually go through stringent quality control procedures to avoid misleading model evaluation results (Blyth et al., 2010; Li et al., 2019; Purdy et al., 2016). Thus, these existing gap-filled data still require processing.

Most importantly, these flux tower datasets lack site-observed vegetation soil, and topography information such as fractional vegetation cover (FVC), Leaf Area Index (LAI), soil texture, slope and aspect. For regional and single-point modeling, the current practice involves deriving these attribute data for LSMs through the inversion of global satellite observations. This raises the uncertainty of LSMs and diminishes the usefulness of flux tower data as benchmarking data for evaluating the model.

Uncertainty in vegetation and soil data constitutes a significant source of uncertainty in LSMs (Dai et al., 2019b; Li et al., 2018). Vegetation composition and density play a prominent part in modulating the surface energy budget (Bagley et al., 2017; Williams and Torn, 2015), by altering canopy conductance, aerodynamic properties, and albedo, ultimately affecting water and energy fluxes between the surface and atmosphere (Anderson et al., 2011; Bonan, 2008). Similarly, soil texture directly affects various soil hydrological and thermodynamic parameters, including saturated soil water content and soil thermal conductivity (Arya and Paris, 1981; Minasny and McBratney, 2007), which have a great impact on soil temperature

65   and moisture, and the terrestrial carbon and water cycle (Dirmeyer, 2011; Entekhabi et al., 1996). Although recent LSM development has attempted to use site-observed attribute data to reduce uncertainty in model results (Harper et al., 2021; Melton et al., 2020), the data used in these studies are typically limited and not publicly available, making it challenging for other researchers to apply these valuable data. Generally speaking, no flux tower dataset can be used directly in the building of LSMs, and they frequently lack the necessary site-observed information about soil, vegetation, and other attributes.

70   To provide more accurate and reliable flux tower data for LSMs modeling and validation, in this study, we conducted thorough quality control for the site data based on the PLUMBER2 dataset produced by Ukkola et al. (2022), resulting in a total of 90 sites. Subsequently, an extensive collection of available flux tower attribute data is carried out, drawing from sources such as site-related literature and websites. The attribute data is further complemented by global data products. In the end, we generated a flux tower dataset that can be directly applied to LSMs and contains essential attribute data. Furthermore,

75   by modeling for the four most important attribute variables—percentage of plant functional type (PFT) cover (PCT_PFT), LAI, canopy height and soil texture—we demonstrate how the site-observed attribute data and the conventional attribute data used by LSMs differ in their model output. These results emphasize the non-negligible impact of flux tower attribute data in model simulation and its development.

2 Data and Methods

80   ### 2.1 Datasets

The data used in this study can be categorized into four groupings, as Table 1 illustrates. Firstly, PLUMBER2 serves as the dataset for data quality screening. The second group is the attribute sources, including 113 site-related literature, 7 flux regional networks, and the Biological, Ancillary, Disturbance, and Metadata (BADM) files provided by FLUXNET and AmeriFlux.

85   The third category includes data sources employed for PFTs classification, incorporating 7 site-related articles, flux tower site measurements of precipitation and air temperature, global maps of the Köppen-Geiger climate classification, and the reprocessed MODIS Version 6.1 Leaf Area Index dataset. The Köppen-Geiger climate classification maps, presented at an unprecedented 1 km resolution, are derived from an ensemble of four high-resolution, topographically corrected climatic maps. They demonstrate higher classification accuracy and substantially more detail than previous versions. And the

90   reprocessed MODIS LAI is much smoother and more consistent with adjacent values, displaying better spatiotemporally continuous and consistency.

Finally, three global datasets were used to complement attribute data of sites lacking site-observed FVC, LAI, and soil texture. LAI complements still use the reprocessed MODIS LAI. FVC complements use a global 300m PFT map, PFT_{local} (Harper et al., 2023). PFT_{local} incorporates a variety of currently available high-resolution satellite data to

95   quantify the percentage of PFT in each 300 m pixel worldwide. The 300m resolution is well-matched with the regional extent of the flux tower footprint (Chu et al., 2021), providing representative FVC data. Complements of soil texture using

the Global Soil Dataset for Earth System Models (GSDE) (Shangguan et al., 2014). The GSDE harmonizes the data collected from various sources and uses a standardized data structure and data processing procedures to derive the final dataset. It is extensively applied in Earth system models (Dai et al., 2019a).

2.2 Processing Methods

We undertook three primary processing steps to establish the final dataset: site and time period selection, attribute collection, and data processing. Firstly, the data selection process involves picking years with a low gap-filled percentage for fluxes (latent and sensible heat) and vapor pressure deficit (VPD), while excluding sites subject to external disturbances and unable to go through EBC. Following that, we collected site-observed vegetation, soil, and topography data. The vegetation attributes included FVC, maximum LAI and mean canopy height. The soil attributes included soil texture, bulk density and organic carbon concentration. The topography attributes included elevation, slope and aspect. Besides, the reference measurement height (for emulating the lowest layer of the atmospheric model to which the LSM would be coupled) was revised by wind speed measurement height if possible. Then, we complemented the vegetation attributes and soil texture using global data. Finally, the FVC was further breakdown to different PFTs. Figure 1 presents a flowchart of the processing pipeline, with each step described in detail below.

Table 1. Summary of the data sources to derive the site attribute dataset.

Data usage	Name	Sources
Site and time period selection	PLUMBER2	Ukkola et al., 2022
Attribute data	Site descriptions in literature (113 articles)	Details in Table S1
	Site regional networks (7 websites)	$AmeriFlux^a$; $AT-Neu\ websit^a$; $ChinaFlux^c$; $European\ Fluxes^d$ $Global\ Monitoring\ Labortatory^e$; $OzFlux^f$; $Swiss\ Fluxnet^g$
	Fluxnet BADM	https://fluxnet.org/
	AmeriFlux BADM	https://ameriflux.lbl.gov/
PFT information	Site descriptions in literature (7 articles)	Details in Table S1
	Site measurements of precipitation and air temperature	Ukkola et al., 2022
	Köppen-Geiger climate classification maps	Beck et al., 2018
	Reprocessed MODIS Version 6.1 LAI dataset	Lin et al., 2023
Data complement	PFT_{local} PFTs maps	Harper et al., 2023
	Reprocessed MODIS Version 6.1 LAI dataset	Lin et al., 2023
	Global soil dataset for earth system models	Shangguan et al., 2014

[a] https://ameriflux.lbl.gov/, [b] http://www.biomet.co.at/, [c] http://www.chinaflux.org/, [d] http://www.europe-fluxdata.eu/,

[e] https://www.gml.noaa.gov/, [f] https://ozflux.org.au/, [g] https://www.swissfluxnet.ethz.ch/.
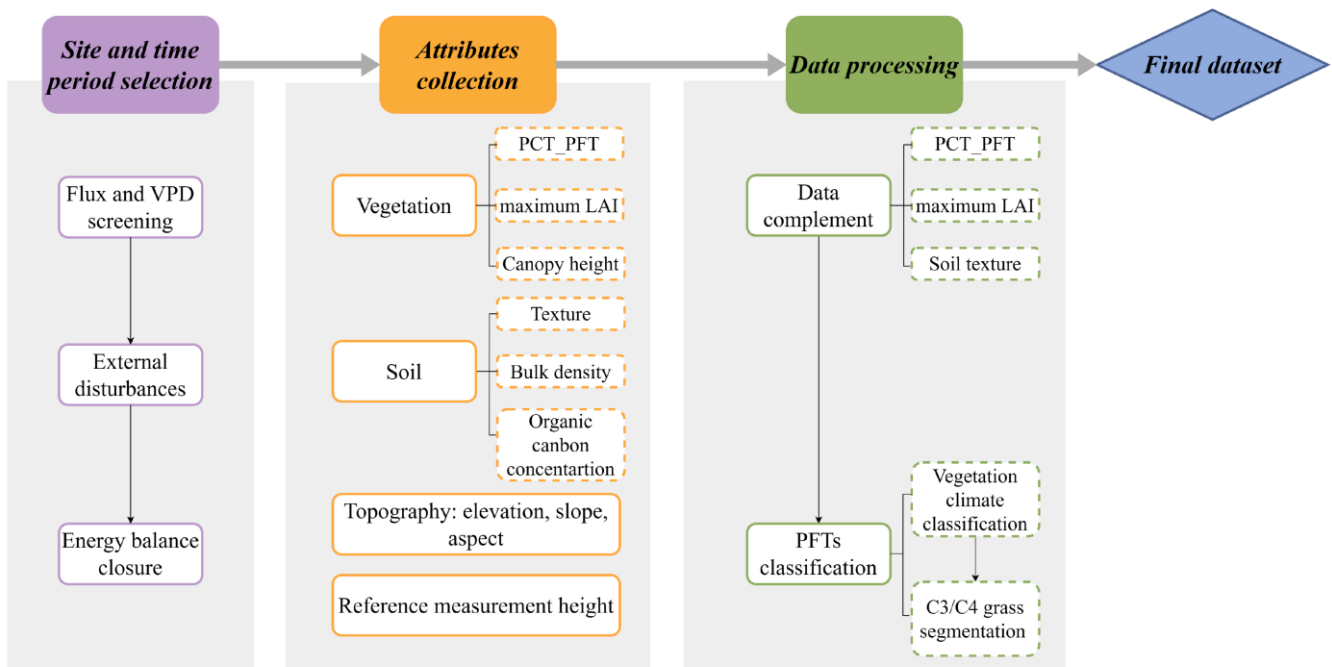
Figure 1. Data flow diagram for the generation of the flux tower attribute dataset.

2.2.1 Site and time period selection

The PLUMBER2 dataset got 170 sites by screening meteorological data. For FLUXNET2015 and La Thuile datasets, specific humidity is not provided in the original data, so it was calculated from VPD (Ukkola et al., 2017). However, the screening process did not take into account the gap-filled situation of VPD. As mentioned earlier, it also did not screen the flux variables. To address these limitations, we further implemented quality control on the PLUMBER2 dataset by performing the following three steps:

1. Sites with only one year of observations were excluded.
2. Selected the years where the proportion of data with fluxes (latent and sensible heat) quality control (QC) ≤ 1 exceeds 90 % (QC = 0 denotes observed data, QC = 1 represents high-quality gap-filled data in FLUXNET2015 and La Thuile, no QC = 1 in OzFlux).
3. Selected the years where the proportion of VPD QC = 0 exceeds 90 % in FLUXNET2015 and La Thuile datasets.

Furthermore, we excluded 23 sites that lacked ground heat flux observations because the EBC correction factor (f_{EBC}) could not be calculated (f_{EBC} = (Rn - G) / (LE + H), net radiation (Rn), ground heat flux (G), latent heat flux (LE) and sensible heat flux (H)). Additionally, two sites were removed as they have a very low energy closure radio (EBR, calculated as (LE + H) / (Rn – G) according to Wilson et al. (2002)) after performing energy closure (sites FR-Lq1 and FR-

Lq2, detailed in Table S3). Lastly, we excluded 10 sites that experienced external disturbances during the observation period, such as irrigation, deforestation, and one site impacted by a sizable body of water. In the end, we preserved non-consecutive years that met the criteria. This allows us to maximize the utility of valuable observational data. Details of the selected and excluded sites and years are displayed in Tables S2 and S3.

2.2.2 Data collection for vegetation attributes

Percent plant functional types cover

FVC data is sourced from site descriptions in literature, regional networks, and FLUXNET BADM files. We looked for appropriate representations of site FVC and obtained site-observed FVC information at 53 sites. We made assumptions in certain sites during the FVC collection to get as much FVC data as possible, addressing scenarios as follows:

1. For sites lacking a direct FVC representation but providing information on the percentage of vegetation flux footprint contribution or dense forest canopy basal area, we also treat them as FVC. Because FVC directly determines this information, and they are close numerically.

2. In the case of grassland and cropland sites, both surface cover landscapes are usually homogeneous cover and manual management. Therefore, we referred to site pictures to make a judgment. If a homogeneous cover could be determined from the pictures, it was assigned a 100 % coverage percentage.

3. There may be seasonal bare soil in some grassland sites with annual vegetation. For these sites, we used the FVC during the peak vegetation growth period.

4. We treated forest litter as if it were grass since bare soil may not be present in forests.

For data completeness, we used the PFT_{local} maps to complement the data for sites lacking site-observed vegetation cover proportion. After that, we further breakdown the FVC data in terms of different PFTs to align with the requirements of LSMs simulation using PFTs. First, trees and shrubs were classified as evergreen or deciduous, as well as coniferous or broadleaf types, based on the vegetation type expressed in the data sources. Next, Köppen-Geiger climate classification maps are employed to categorize the climate type of PFTs using the method proposed by Poulter et al. (2011). To better represent the C3 and C4 grasses, we prioritize segmentation based on the data source descriptions. If site description was not available, then segmentation was performed using the Still et al. (2003) method, which uses flux tower air temperature, precipitation, and reprocessed MODIS Version 6.1 LAI.

A total of 16 PFTs includes the full set of 15 PFTs initially developed by Bonan et al. (2002) supplemented with a new bare soil surface type. The full set of PFTs includes bare soil; Needleleaf evergreen tree, temperate (ENT_Te); Needleleaf evergreen tree, boreal (ENT_Bo); Needleleaf deciduous tree (DNT); Broadleaf evergreen tree, tropical (EBT_Tr); Broadleaf evergreen tree, temperate (EBT_Te); Broadleaf deciduous tree, tropical (DBT_Tr); Broadleaf deciduous tree, temperate (DBT_Te); Broadleaf deciduous tree, boreal (DBT_Bo); Broadleaf evergreen shrub, temperate (EBS_Te); Broadleaf deciduous shrub, temperate (DBS_Te); Broadleaf deciduous shrub, boreal (DBS_Bo); C3 grass, arctic; C3 grass; C4 grass; Crop. This PFTs classification scheme is widely utilized in LSMs.

Maximum leaf area index

165 Maximum LAI data is sourced from site descriptions in literature and AmeriFlux BADM files. Included are the explicitly stated maximum LAI and the maximum LAI acquired from interannual scatterplots. Similarly, we made assumptions in certain sites to get as much data as possible. Specifically, the summertime LAI observation is used as the maximum LAI. And we accept LAI to be maximum when the LAI value for a single site is provided without observation time or additional supporting information. To distinguish such instances, we have positioned quality control flags in the final dataset. Users are

170 free to select based on how accepting they are. A total of 67 site observations of maximum LAI were collected, with 33 of these sites providing information on the year of observation. For data completeness, we used the reprocessed MODIS Version 6.1 LAI dataset to complement the data for sites in case of site-observed maximum LAI was unavailable.

Canopy height

We calculated the mean canopy height over the observation period for 69 sites included in FLUXNET2015 dataset, using the

175 canopy heights reported in FLUXNET BADM file across different periods. The mean canopy height provides a more truthful representation of the vegetation condition during the period of observation. For the remaining 21 sites, the canopy height provided by PLUMBER2 was used.

2.2.3 Data collection for soil attributes

Soil texture

180 Soil texture data is sourced from site descriptions in literature, regional networks, and AmeriFlux BADM files. These descriptions encompass both explicitly stated the percentages of sand, silt, and clay and the different types of soil textures, such as sandy loam. The latter does not directly give the percentages of sand, silt, and clay. So, we referred to the soil composition table shown by Dy and Fung (2016), enabling the derivation of specific proportions. The table classifies soil into 16 categories based on the proportions of sand, silt, and clay. In total, 72 site observations of soil texture were collected,

185 with 34 supplying information on the depth of observations. For data completeness, we used the GSDE dataset to complement the data for sites lacking site-observed soil texture.

Soil bulk density and organic carbon concentration

Soil bulk density and organic carbon concentration data are sourced from site descriptions in literature, regional networks, and AmeriFlux BADM file. Specifically, soil bulk density data were collected at 37 sites, and soil organic carbon

190 concentration at 23 sites. At 32 and 22 sites, respectively, the observation depth was given. Despite the scarcity of site-observed data for these two soil attributes, we have included them in the final dataset. For site-specific studies, they can provide useful references for researchers.

2.2.4 Data collection for topography attributes

The topography data encompasses site elevation, slope and aspect. These data are gathered from site descriptions in literature,

195 regional networks, FLUXNET and AmeriFlux BADM files. Specifically, we acquired elevation for 89 sites, slope for 57

sites, and aspect for 49 sites from these reference sources. In the AU-Lit site, where site elevation data was unavailable from the aforementioned references, we used the elevation given in Ukkola et al. (2022).

2.2.5 Reference measurement height

Site descriptions in literature, regional networks, FLUXNET and AmeriFlux BADM files are all sources of the reference
200   measurement height. From these sources. we look for the height of wind speed measurement or the height of instrument used to wind speed measurements (such as the wind cup). In instances where flux tower meteorological observation equipment lacks an individual wind speed observation apparatus, we suppose the use of three-dimensional sonic anemometer for wind speed measurements. As a result, wind observation heights are available for a total of 76 sites. For the remaining 14 sites where wind observation heights were not reported, we used flux observation height as a substitute.

205   ### 2.3 Modeling assessment of attribute data

The impact of collected attributes on carbon, water, and energy fluxes is assessed through single-point simulations using the Common Land Model (CoLM) (Dai et al., 2003). We used its latest version, CoLM202X (https://github.com/CoLM-SYSU/CoLM202X/tree/master, last access: 21 November 2023). Here, the simulations aim to evaluate the discrepancies in model results between using attributes observed at the site and commonly utilized by LSMs. For simplicity, we refer to site-
210   observed data as "site data" and data commonly utilized by LSMs as "default data" in subsequent descriptions. We focus on the four most essential attributes, PCT_PFT, LAI, canopy height and soil texture, to demonstrate their corresponding impacts.

The default data generally rely on global LAI and soil texture mapping products, lookup table canopy height, and site IGBP (International Geosphere–Biosphere Programme) classifications to characterize surface vegetation and soil conditions. In this study, the default LAI and soil texture refer to the reprocessed MODIS version 6.1 LAI and GSDE soil texture as
215   shown in Table 1. Lookup table canopy heights are sourced from CoLM, while site IGBP classifications are obtained from FLUXNET and OzFlux. We chose ten sites for each of the attributes—LAI, canopy height, and soil texture—where site data differ the most from default data (In the lookup table canopy height simulations, sites with zero plane displacement exceeding reference measurement height are excluded.). For PCT_PFT analyses, sites with IGBP types that are a combination of trees and grasses (OSH, WSA, SAV) were chosen, resulting in six available sites. These sites were simulated
220   to show the respective impact of different attributes in model results. Table 2 provides an overview of the chosen sites along with their corresponding attribute information.

At each site, we run CoLM at either half-hourly or hourly resolution, depending on the data available, for all years in the original dataset. Subsequent analyses are conducted exclusively for the years we have chosen. To reach an equilibrium in soil moisture and temperature, the first year of atmospheric forcing data was cycled. CoLM was recursively run at each site
225   using a 20-year spin-up. The discrepancy of site data relative to default data is compared by an ensemble of climate-related variables, including latent heat (LE), sensible heat (H), net radiation (Rn), upward shortwave radiation (SWup), gross primary production (GPP), friction velocity (Ustar), surface(0-4.5cm) soil water content (SWC), and total runoff (TR).

To quantify differences between output from the site and default data, and considering the seasonal fluctuations in the impacts of soil and vegetation on climate-related variables (Dirmeyer, 2011; Forzieri et al., 2020). We designed a statistical

230 indicator called the percentage of mean difference (MD %) (Eq. 1), which is calculated as the mean difference in each month expressed as a percentage of the observed or default modeled mean for the year. Multi-year average time series are used here to capture more stable differences in output. In addition, we used delta root mean squared error (ΔRMSE) (Eq. 3) and Δ|Bias| (Eq. 5) to measure the difference in RMSE and Bias of the output between site and default data, enabling us to assess the model's performance after using site data.

235
$$MD\ \% = \begin{cases} \dfrac{|\frac{1}{n}\sum_{i=1}^{n}(Mod_{site,i} - Mod_{default,i})|}{\frac{1}{365}\sum_{j=1}^{365} Obs_j}, & for\ LE, H, Rn, SWup, GPP, and\ Ustar \\[4mm] \dfrac{|\frac{1}{n}\sum_{i=1}^{n}(Mod_{site,i} - Mod_{default,i})|}{\frac{1}{365}\sum_{j=1}^{365} Mod_{default,j}}, & for\ SWC\ and\ TR \end{cases} \tag{1}$$

$$RMSE = \sqrt{\frac{\sum_{i}^{n}(Mod_i - Obs_i)^2}{n}} \tag{2}$$

$$\Delta RMSE = RMSE_{site} - RMSE_{default} \tag{3}$$

$$Bias = \frac{\sum_{i}^{n}((Mod_i - Obs_i)}{n} \tag{4}$$

$$\Delta|Bias| = |Bias_{site}| - |Bias_{default}| \tag{5}$$

240 Where $Mod_{site,i}$ and $Mod_{default,i}$ are the predicted value using site data and default data, respectively. Obs_j is observed value. n is the number of paired values. $RMSE_{site}$ and $RMSE_{default}$ are the RMSE of the simulation results using site data and default data, respectively. $Bias_{site}$ and $Bias_{default}$ also correspond to the Bias in these results.

245

250

Table 2. Selected sites and their attribute values used in the modeling assessment for attribute data. The suffix "default" is for model default data, and the "site" represents site data.

Site	LAI_default[a] (m²/m²)	LAI_site[b] (m²/m²)	Site	TEX_default[c]	TEX_site[b]
US-KS2	6.6 (2005[e])	2.7 (2005)	IT-Cpz	33/45/22	87/8/5
DK-Lva	3.1 (2004)	6.9	DE-Gri	52/29/20	10/81/9
DE-Bay	3.6	6.5	FI-Sod	52/25/20	92/5/3
US-Goo	4.5	2.0	ES-LMa	49/24/24	80/11/9
DE-Seh	3.2 (2009)	5.9 (2009)	AU-Cpr	64/18/18	94/4/2
US-GLE	1.5	3.8	SD-Dem	67/18/14	96/4/0
US-Moz	6.1 (2006)	4.0 (2006)	CZ-wet	39/37/32	10/85/5
DE-Gri	6.5 (2004)	4.4 (2004)	AU-DaP	63/18/19	92/5/3
IT-Cpz	5.4	3.5	AU-DaS	63/12/25	92/5/3
US-MMS	7.0	5.2	IT-SRo	69/17/15	95/4/1
Site	H_{can}**_default[d] (m)**	H_{can}**_site[b] (m)**	**Site**	**IGBP**	**PCT_PFT_site[b]**
IT-Cpz	35	14.3	AU-How	WSA	EBT_Tr/DBS_Te/C4 : 50/25/25
BE-Vie	17	33.7	ES-LMa	SAV	EBT_Te/C3 : 20/80
AU-Lit	35	20.0	SD-Dem	SAV	EBT_Tr/C3/C4 : 10/27/63
DE-Hai	20	33.9	US-SRM	WSA	DBS_Te/C3/C4 : 35/43/22
IT-Ren	17	29.0	US-Ton	WSA	EBT_Te/C3 : 40/60
DE-Tha	17	28.4	US-Whs	OSH	Bare/DBS_Te/C3 : 39/51/10
IT-Lav	17	28.0			
US-Ton	20	9.9			
RU-Fyo	17	26.3			
CH-Dav	17	25			

255   [a] The maximum LAI at the pixel containing the site provided by Reprocessed MODIS version 6.1 LAI. [b] Site-observed data collected in this study. [c] Soil texture (sand/silt/clay) at the site location extracted from the GSDE dataset. [d] Canopy height of the dominant vegetation type at the site from the CoLM lookup table. [e] Specific year of maximum LAI.

(a)
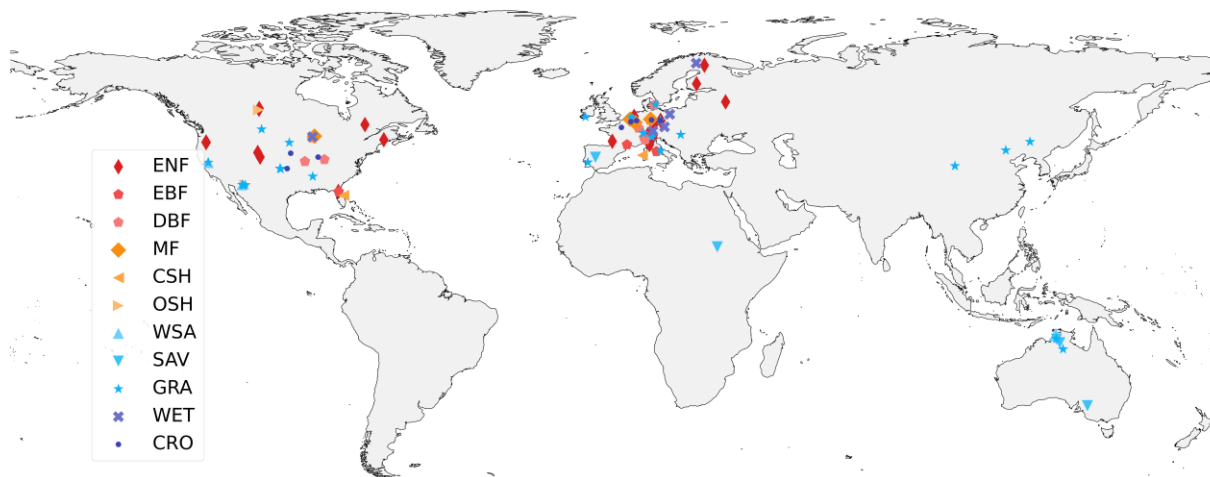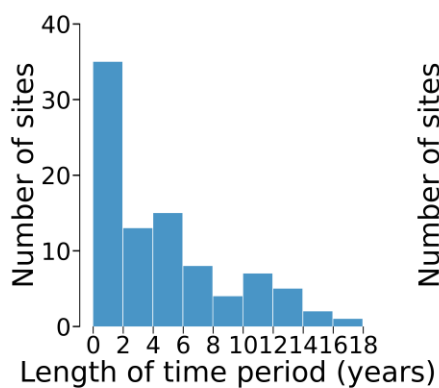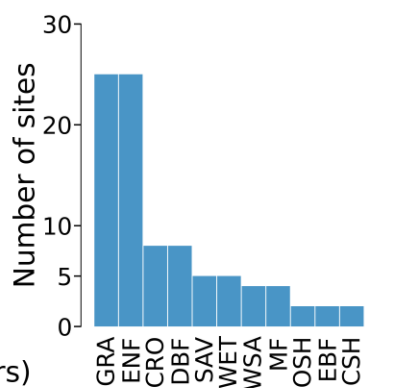
(b) (c) (d)
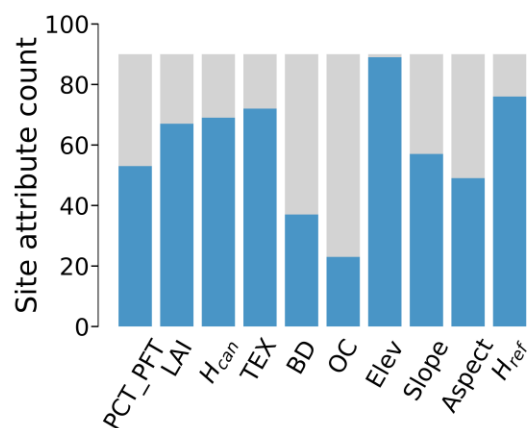
Figure 2. Summary of selected sites and collected site-observed attribute data. (a) A map of selected sites and their IGBP types. (b) A histogram of site numbers for selected sites. (c) Number of selected sites per IGBP vegetation class. (d) Number of collected site-observed attribute data for PCT_PFT, maximum LAI (LAI), mean canopy height (H_{can}), soil texture (TEX), bulk density (BD) and organic carbon concentration (OC), elevation (Elev), slope, aspect, and wind reference measurement height (H_{ref}).

3 Results

3.1 Global distribution and attribute information of selected sites

The final dataset contains 90 globally distributed sites (Fig. 2a). The majority are in North America and Europe, followed by Australia, with smaller representations in Asia (3 sites) and Africa (1 site). Temporal coverage spans from 1997 to 2017, totaling 475 site years. Individual site observations range from 1 to 17 years, with a median of 4 years (Fig. 2b). Despite a reduction in available sites and years due to thorough quality control, the dataset does offer reliable meteorological forcing and flux assessment data for LSMs. Furthermore, 90 sites encompass the full range of IGBP classifications originally presented, cover a wide spread of biomes, from grasslands and savannas to forest ecosystems (Fig. 2c). This enables users to evaluate models across various biomes using quality-benchmarked flux tower observations.

Out of the 90 sites, data were collected on the PCT_PFT for 53 sites, maximum LAI for 67 sites, average canopy height for 69 sites, soil texture for 72 sites, soil bulk density for 37 sites, concentration of soil organic carbon for 23 sites, elevation for 89 sites, slope for 57 sites, aspect for 49 sites, as well as wind observation height at 76 sites (Fig. 2d). In the absence of site-observed PCT_PFT, TEX, and LAI, we opted for appropriate global data to complement them for data completeness. To improve data utilization, we offer the observation year of maximum LAI and the depth of soil texture, which were availed at 33 and 34 sites, respectively.
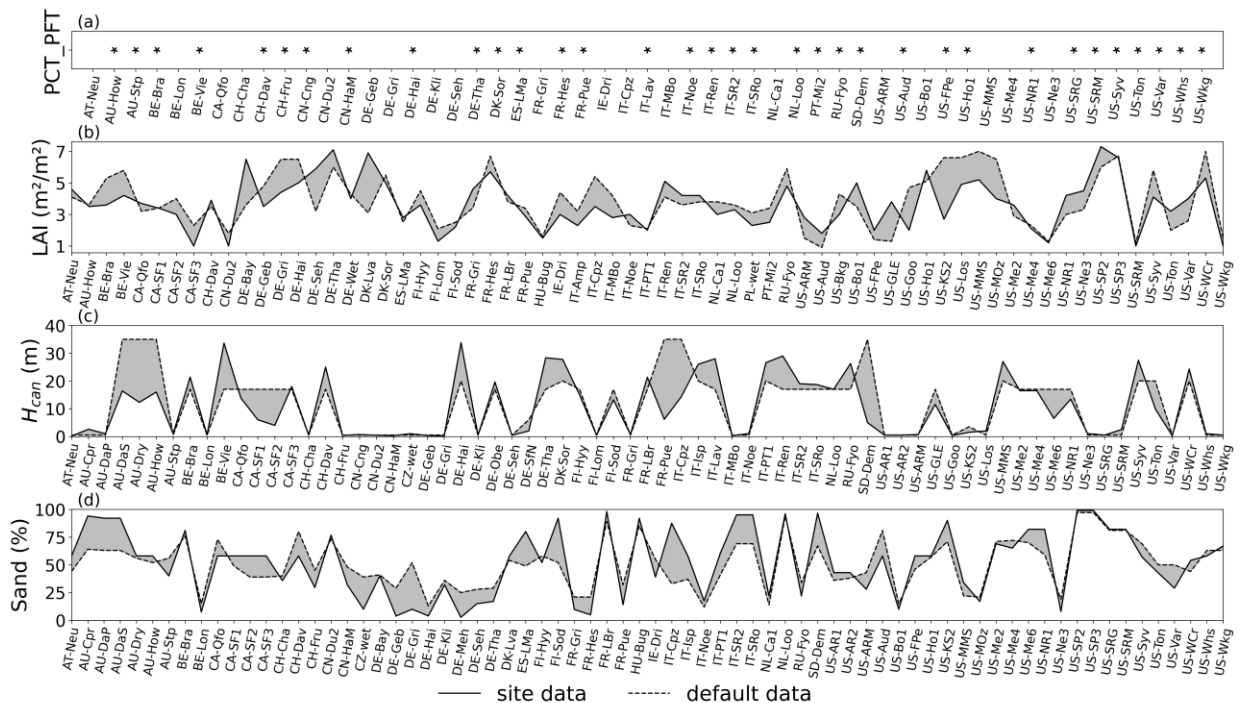
Figure 3. The discrepancies between site data and default data of (a) PCT_PFT (the asterisk indicates non-single PFTs), (b) maximum LAI, (c) canopy height (H_{can}), and (d) the percentage of sand.

Figure 3 depicts the discrepancies between site data and default data for PCT_PFT, maximum LAI, canopy height, and soil texture. The PCT_PFT has non-single PFTs at 34 sites, offering a more accurate representation of the vegetation conditions compared to IGBP classifications. As for LAI, canopy height, and soil texture, variations between site data and default data are substantial in certain sites. Specifically, at 31 sites, there is a discrepancy in LAI values exceeding 1 m^2/m^2, and canopy height differing by over 10 meters at 15 sites, with the disparity in sand % exceeding 20 % at 18 sites.

3.2 The flux tower site attribute dataset

The final dataset is formatted in NetCDF (Network Common Data Form). Table 3 outlines the attribute variables and corresponding supporting descriptions for each site in the file. These attributes can be categorized into vegetation, soil, and topography attributes, reference heights, and filtered high-quality years.

For the maximum LAI, the file furnishes the range of years for maximum LAI, and the maximum for a specific year. Regarding three soil attributes, soil texture, bulk density, and organic carbon concentration, the file provides attribute values for multiple soil layers and gives the specific depth of their corresponding soil layer.

Concerning reference height, we give its corresponding observed variable, i.e., wind speed or fluxes (latent and sensible heat). Additionally, the NetCDF file incorporates reference sources for each attribute. These sources are included to facilitate access to the original data and flexibility in application. A comprehensive summary of these reference sources is provided in Table S1.

Table 3. Attribute variables and auxiliary descriptions provided in the final dataset (note that not all sites provide 'Soil_BD', 'Soil_OC', 'Slope', and 'Aspect').

Variable (Dimension)	Long name	Unit	Description
PCT_PFT (pft=16)	Percent plant functional types cover	%	Source[a];
LAI_Max	Maximum leaf area index	m^2/m^2	Source; year_range[b]; LAI_Max_year[c]
Canopy_height	Canopy height	m	Source;
Soil_TEX (particle_size=3, soil_layer=4)	Soil texture(sand/silt/clay)	%	Source; layer_n_depth[d]
Soil_BD (soil_layer=4)	Soil bulk density	g cm^{-3}	Source; layer_n_depth[d]
Soil_OC (soil_layer=4)	Soil organic carbon concentration	%	Source; layer_n_depth[d]
Elevation	Site elevation	m	Source;
Slope	Site slope	-	Source;
Aspect	Site aspect	-	Source;
Reference_height	Measurement height of wind speed or flux	m	Source; Measurement variable (Wind or Flux)
year_qc (year=21)	Selected year of high-quality data	-	-

[a] The sources of collected attribute data. [b] Range of years with maximum LAI. [c] Maximum LAI for specific year. [d] The "n" ranges from 1 to 4, denoting the four soil layers in ascending order of depth. The parameter "layer_n_depth" indicates the depth of respective "soil layer", corresponding to the depth at which soil data is observed.

3.3 Impact of site attributes on modeling

305   The impacts of altering land surface representation from default data to site data, quantified by MD %, on LE, H, Rn, SWup, GPP, Ustar, SWC, and TR are shown in Fig. 4. It distinctly demonstrates how vegetation and soil components affect carbon, water, and energy to varying degrees, contingent on the season. The influence of vegetation cover, soil texture, and LAI on LE and H is primarily felt in the spring and summer. The opposite was true for canopy height, which produced the most substantial effects in autumn and winter. The impact of vegetation cover on Rn and SWup remains more consistent

310   throughout the year, whereas LAI maintains a more pronounced effect in spring and summer. In terms of GPP, attribute factors play a more significant role during the summertime. But the effects of vegetation and soil on Ustar appear to be independent of season. For SWC and TR, both are predominantly influenced by soil texture. The difference is that soil texture significantly affects SWC across all seasons, whereas its impact on TR occurs primarily during the summer and fall. Additionally, it was noted that vegetation cover could have a significant change on TR. This is due to the salient impact at

315   the SD-Dem site, situated within the African savannah with an average annual precipitation of 320mm (Ardö et al., 2008).

To elucidate the magnitude of each attribute's impact on different variables, figure 5 further displays the monthly average maximum MD %. On average, the impacts of four attributes—PCT_PFT, LAI, canopy height, and soil texture—on LE and H were comparatively equilibrated. Their monthly average maximum MD % on H are all in the range of 15-30 %. And the effect of soil texture on LE is relatively significant, at 17.5 %. Moving on to Rn, vegetation cover emerges as the

320   chief influencer with a monthly average maximum MD % of 8.5 %. In contrast, SWup is heavily dictated by LAI, at 52.8 % because of the exceptionally high value at the US-GLE site. The vegetation cover and LAI, with a monthly average maximum MD % of more than 50 %, dominate the changes of GPP. Since soil texture affects permeability, aeration, and the ability of the soil to hold water and nutrients, it also has a visible impact on GPP. On the other hand, Ustar is almost exclusively shaped by vegetation cover and canopy height. This makes sense because the intensity of land-atmosphere

325   exchange in vegetated areas is directly tied to canopy height, and changes in vegetation cover typically correspond to changes in canopy height. Concerning SWC and TR, vegetation cover and soil texture are two crucial attributes. Soil texture exhibited monthly average maximum MD % of 46.8 % and 147.9 % for each, while vegetation cover showed 22.6 % and 278.8 %, respectively.

Figure 6 uses ΔRMSE and Δ|Bias| to show the shifts in model performance using site data. The incorporation of site-

330   observed attribute data significantly improves the simulation of Rn, SWup, and Ustar. Specifically with respect to individual attributes, the PCT_PFT proves helpful for modeling both Rn and SWup. Concurrently, the inclusion of site LAI also contributes to the enhancement of SWup. Enhancements to these fundamental energy terms contribute to more accurate modeling of latent and sensible heat. Furthermore, the use of site LAI and canopy height demonstrates steady improvements on GPP and Ustar, respectively.

335   In summary, these results underscore the significant impact and importance of incorporating site-observed attribute data in the simulation of carbon, water, and energy fluxes in LSMs.
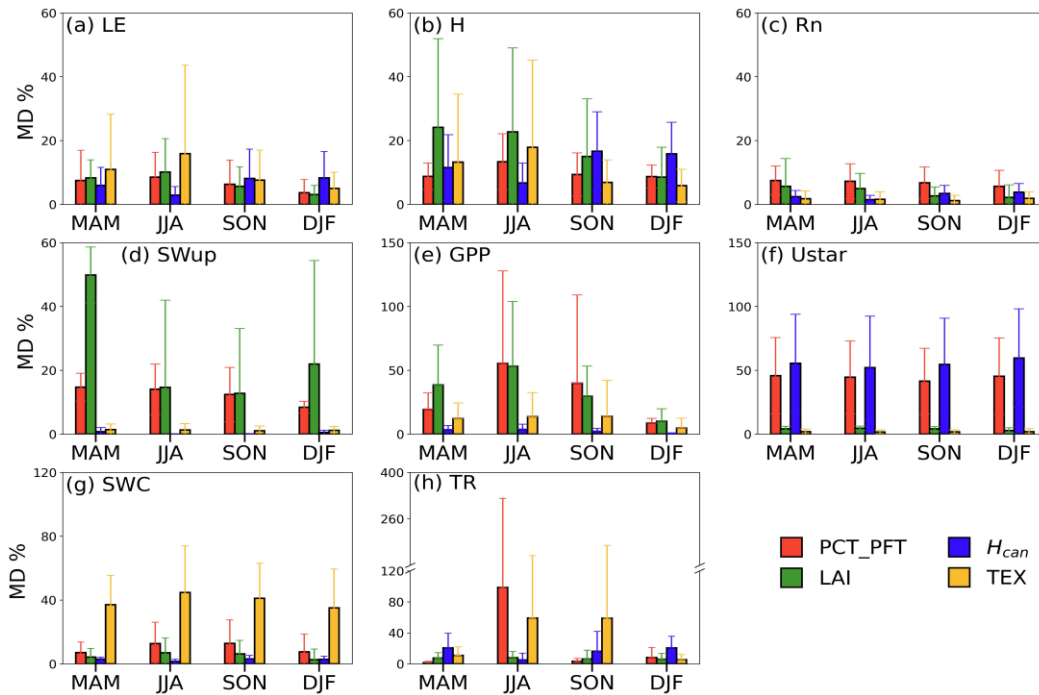
Figure 4. The percentage of mean difference (MD %) of PCT_PFT, LAI, canopy height (H_{can}) and soil texture (TEX) on LE, H, Rn, SWup, GPP, Ustar, SWC and TR for each season, respectively. The error bars indicate a standard deviation from the multi-site mean. Monthly adjustments for southern hemisphere sites in calculations, to ensure consistency between seasons and months in multi-site averaging (i.e., DJF are considered to be JJA, MAM are considered to be SON, and so on.).
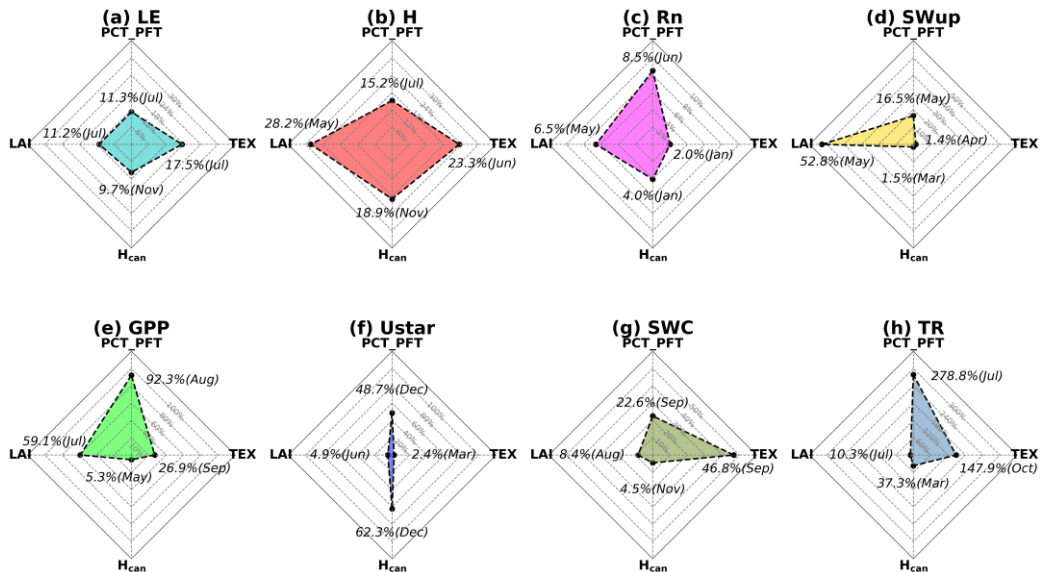
Figure 5. The monthly average maximum MD % of PCT_PFT, LAI, canopy height (H_{can}) and soil texture (TEX) on LE, H, Rn, SWup, GPP, Ustar, SWC and TR, respectively. The month with the maximum is indicated in parentheses.
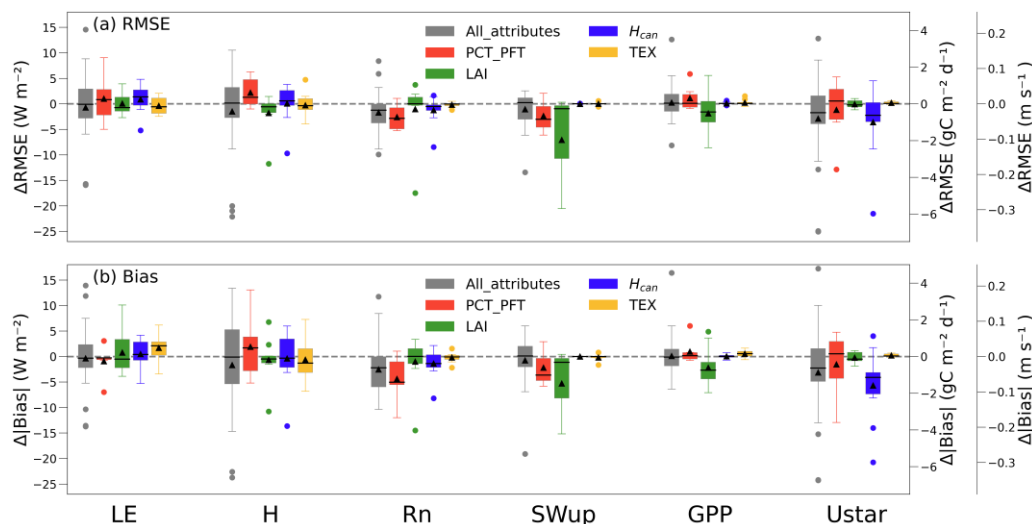
345

Figure 6. Box plot of changes in RMSE (ΔRMSE) and absolute Bias (Δ|Bias|) when using site data versus default data. PCT_PFT, LAI, H_{can} (Canopy height), and TEX (soil texture) denote the individual impacts of the four attributes. All_attributes represent the changes produced by four attributes together across the 36 sites selected. Boxes (25th and 75th percentiles) and whiskers (5th and 95th percentiles), with median (black line) and mean (black triangle). Solid circles denote

350 outliers for values greater than 1.5 times the interquartile range from the nearest 25th or 75th percentile.
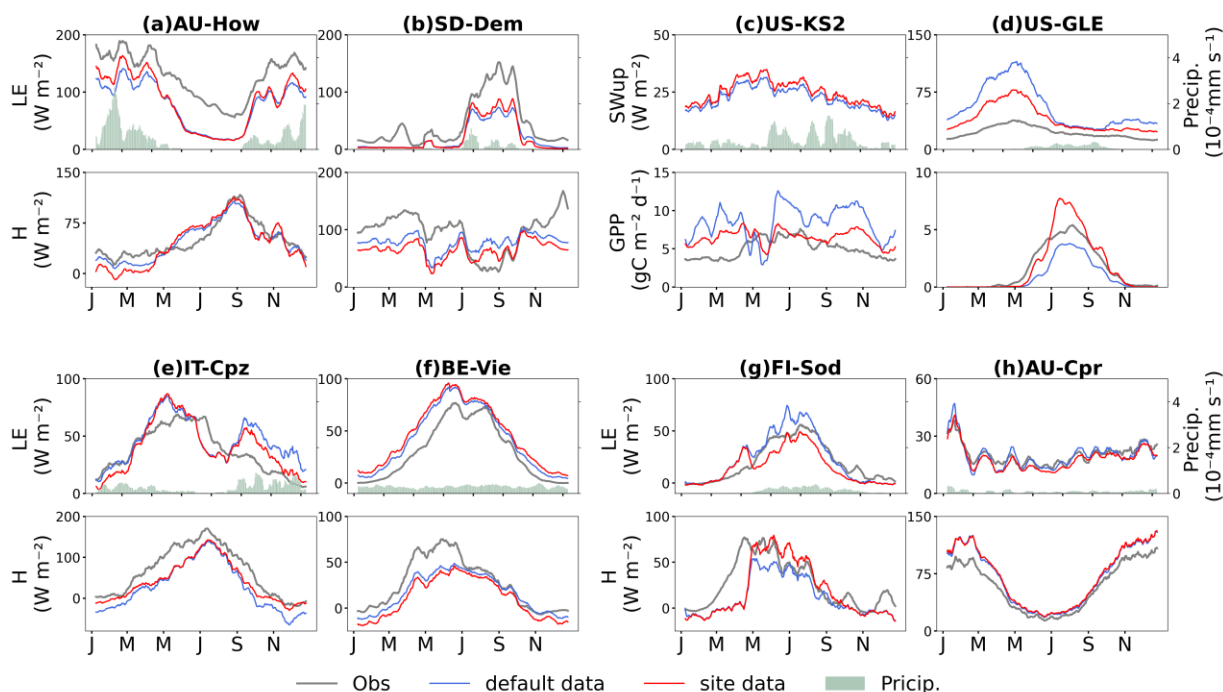
Figure 7. Multi-year daily average of the seasonal cycle of model (default, site) and observed LE, H, SWup, and GPP at 8 selected sites, smoothed with a 14-day moving average for clarity.

4 Discussion

355 In land surface community, flux tower attribute data is currently not given enough attention. Here, we have acquired 90 sites with dependable quality by comprehensive selection, and provided data on vegetation, soil, and topography attributes observed at the site. Through single-point simulations, we illustrated their indispensable role in LSM development. Accurate attribute data will provide multiple benefits by lowering uncertainty in model single-point calibration and evaluation.

After selection, fewer sites and years are available. However, the retained data offers trustworthy observations that can

360 be directly applied. Data quality is generally the focus of model calibration and evaluation, and developing LSMs can benefit immensely from the usage of a modest number of sites (Brooke et al., 2019; Harper et al., 2021; Swenson et al., 2019). These updates will therefore help the model's evolution. To collect more site-observed attribute data, while taking into account the diversity described within the same attribute data, particularly the percentage of vegetation cover. We made a few approximations and assumptions in the data collection procedure. Although these methods may introduce slight

365 deviations from the genuine values, they do a good job of reproducing the surface conditions of these sites. Furthermore, we provide descriptions of the attribute data as detailed as possible. For instance, the year and depth of observation are given along with the maximum LAI and soil texture whenever feasible, respectively. They are valuable references for data applications. One might argue that the auxiliary descriptions are just as important as the attribute data itself.

Using CoLM at 36 sites, we evaluated the impacts of PCT_PFT, LAI, canopy height, and soil texture on model results.

370 What is conducted here is not an ideal experiment, but rather an actual demonstration of the discrepancies in model results between site data and default data. According to the results, which are in line with earlier research (Dai et al., 2019b), vegetation cover appreciably affects each of the eight variables examined. And among the four attributes, net radiation was the most affected by vegetation cover (Fig. 5). This is due to the cover of plants being the most noticeable surface feature, directly changing surface energy absorption. The net radiation simulation was enhanced using the site PCT_PFT, but the

375 latent and sensible heat did not perform as well. This may be related to the model's previous development and evaluation, which was mostly centered on the IGBP classifications (Dai et al., 2019c; Zhang et al., 2017; Zhu et al., 2017). Notably, unit LAI variations elicit more substantial fluctuations in fluxes at lower LAI values (usually less than 2 m^2/m^2), according to Launiainen et al. (2016). In light of that, all of the sites we chose have LAI values greater than 2 m^2/m^2, except US-GLE, the impact of LAI obtained here are relatively minor.

380 Additionally, we find that the impact of attributes is substantially associated with precipitation. As illustrated in the average seasonal cycle shown in Fig. 7, the AU-How site in Australia along with ample rainfall during wet season, and the increase in surface available energy due to vegetation cover brings about a significant increase in LE. In contrast, since limited water is available for evapotranspiration at the SD-Dem site, H is the primary feedback from changes in surface energy. The results from the US-KS2 and US-GLE sites indicate that the growing season, synchronized with water

385 availability, is when LAI exerts a major influence on GPP. And a notable variation in SWup was seen at the US-GLE site, attributed to the presence of snow cover (Berryman et al., 2018). Corrections to LAI can improve the simulation by reducing

albedo inaccuracies. This corroborates the Essery (2013) point that inadequate land-cover data was largely to blame for the uncertainty in the climate–snow albedo feedback in LSMs. Results from the IT-Cpz and BE-Vie sites suggest that differences in the intensity of land-air exchange, caused by variations in canopy height, are truly reflected in LE during the
390   rainy season. Regarding soil texture, a comparison of results between FI-Sod and AU-Cpr sites revealed stronger control of LE by soil texture during the period of high precipitation intensity. This is partly attributed to increased water availability and largely to the full realization of differences in soil infiltration capacity under high-intensity precipitation.

A previous study viewed that attribute data have little effect on model results (Ménard et al., 2015). Its study, however, may lack representativeness since it was limited to one site. Furthermore, it averaged differences resulting from attribute data
395   across the whole time series, by using the raw RMSE and correlation coefficient statistics metrics. This does make it difficult to detect the crucial role of attribute data. As described in Sect. 3.3, the impacts of attribute data on climate-related variables occur mostly during the growing season.

By combining multiple data sources, we were able to maximize the available site-observed attribute data. Nevertheless, the data sources were published works, leading to deficiencies for certain sites. And the attribute data we collected focused
400   on fundamental soil and vegetation information. Future endeavors will call for the incorporation of additional surface parameters, such as irrigation, wildfire, and the depth of soil moisture and vegetation root, which are demanded for LSMs. These collections of site attributes are low-cost but would strongly benefit model enhancement. In addition, the impact of attribute data on model results was simulated using one model, potentially limiting the representativeness of our findings.

As LSM continually advances its scheme and process, an increasing array of surface parameters will be incorporated,
405   elevating the model to a heightened level of sophistication. It is imperative that these parameters be clarified. Working with site-observed attribute data enabled us to narrow down reasons for model biases, facilitating perception of the authentic feedback with diverse schemes and processes.

5 Data availability

The flux tower site attribute dataset provides comprehensive filtered high-quality years, site-observed vegetation, soil,
410   topography attributes, and reference measurement height. Each site's data is formatted within a NetCDF file named according to the site name, database, and attributes (vegetation, soil, topography, and reference height), such as 'AT-Neu_FLUXNET2015_Veg_Soil_ Topography_ReferenceHeight.nc'. The dataset comprises a total of 90 NetCDF files and can be accessed at Zenodo under https://doi.org/10.5281/zenodo.10939725 (Shi et. al., 2024).

6 Code availability

The processing codes are available at https://github.com/Mbnl1197/Flux-tower-attribute-for-LSM (last access: 2 March 2024) (DOI: https://doi.org/10.5281/zenodo.10939950; Shi et. al., 2024)

7 Conclusions

This study is centered on two issues with utilizing flux tower data in LSMs, including inadequate quality of data and insufficient site attribute data. We performed a comprehensive quality control on flux tower data. Through the examination of observation percentage, energy balance closure, and external disturbances, 90 high-quality flux tower sites with 475 site years were produced. Combining various data sources, we created a flux tower attribute dataset through data collection, processing, and complementarity. The site-observed PCT_PFT, maximum LAI, mean canopy height, soil texture, bulk density and organic carbon concentrations, site elevation, slope and aspect were collected, and wind speed measurement height was acquired.

Furthermore, the attribute data collected in this study and frequently used by LSMs are incorporated in single-point modeling respectively, aimed at quantifying the differences in model output. Our results demonstrate the significance of certain attributes in the variation of specific variables. All four attributes significantly influence both latent and sensible heat. Their monthly average maximum MD % typically ranges from 10 % to 30 %. Vegetation cover and LAI serve as the primary controls for net radiation and upward shortwave radiation, respectively, with monthly average maximum MD % of 8.5 % and 52.8 %. Both GPP and Ustar were strongly influenced by vegetation cover, with LAI and tree height also exerting significant effects on GPP and Ustar, respectively. The monthly average maximum MD % for each of these impacts exceeds 50 %. For hydrologic variables, i.e., SWC and TR, soil texture typically holds greater significance, followed by vegetation cover. We reveal that the magnitude of these differences is usually accompanied by seasonal fluctuations. Particularly regarding fluxes and GPP, greater discrepancies are generally discerned during spring and summer. These results stress the necessity of site-observed attribute data in the development of LSMs.

Our endeavors mitigate the inadequacies of flux tower attribute data, elevating the ability of flux tower data to serve as benchmarking data for LSMs. The dataset provides relatively complete site attribute data and high-quality flux validation data, which can be directly used as inputs and simulation validation for LSMs. This facilitates the comparison of LSM simulations under the same standard framework, promoting their development. Moreover, this effort will draw more attention to flux tower attribute data from the land surface modeling community and foster communication between ecology and modeling.

Author contributions

Conceptualization: H.Y.; Data curation: H.Y. and J.S.; Formal analysis: J.S., H.Y., W.D. and W.L.; Funding acquisition: H.Y. and Y.D.; Investigation: H.Y. and J.S.; Methodology: H.Y., J.S., N.W., Z.W. and S.L.; Resources: Y.D. and H.Y.; Software: J.S., H.Y., H.L., W.L., N.W., J.Z. and H.Z.; Validation: H.Y., Z.L., W.D., W.L., S.Z. and X.L.; Visualization: J.S.; Writing – original draft preparation: J.S.; Writing – review & editing: J.S., H.Y., Z.W., W.L., W.D., Z.L. and Y.D. All authors have read and agreed to the published version of the manuscript.

Competing interests

The authors declare that they have no conflict of interest.

Acknowledgements

We thank Anna M. Ukkola for her solid work in flux tower data processing, which provided a robust foundation for our research. We are also grateful for her responsiveness to our questions in using PLUMBER2. We extend our thanks to Danielle Svehla Christianson of Integrated Data Systems, Scientific Data Division, and Lawrence Berkeley National Laboratory for her prompt assistance in utilizing AmeriFlux BADM data. This work accessed several flux tower networks in the FLUXNET community, including AmeriFlux, ChinaFlux, European Fluxes, OzFlux, and Swiss Fluxnet. Special thanks to FLUXNET and AmeriFlux for providing the BADM data. We also accessed data from ESRL's Global Monitoring Laboratory (GML) of the National Oceanic and Atmospheric Administration (NOAA) and the AT-Neu site research group. This work is based on numerous publications, we thank these scientists for sharing their data. The PFT_{local} maps were supported and provided by the ESA CCI Land Cover project. The Köppen-Geiger climate classification maps are hosted by GloH2O.

Financial support

This work was supported by the Natural Science Foundation of China (under Grants 42075160 and 42088101), Guangdong Major Project of Basic and Applied Basic Research (2021B0301030007), the Southern Marine Science and Engineering Guangdong Laboratory (Zhuhai) (No. SML2023SP216) and the specific research fund of The Innovation Platform for Academicians of Hainan Province (YSPTZX202143).

References

Anderson, R. G., Canadell, J. G., Randerson, J. T., Jackson, R. B., Hungate, B. A., Baldocchi, D. D., Ban-Weiss, G. A., Bonan, G. B., Caldeira, K., Cao, L., Diffenbaugh, N. S., Gurney, K. R., Kueppers, L. M., Law, B. E., Luyssaert, S., and O'Halloran, T. L.: Biophysical considerations in forestry for climate protection, Frontiers in Ecol & Environ, 9, 174–182, https://doi.org/10.1890/090179, 2011.

Ardö, J., Mölder, M., El-Tahir, B. A., and Elkhidir, H. A. M.: Seasonal variation of carbon fluxes in a sparse savanna in semi arid Sudan, Carbon Balance Manage, 3, 7, https://doi.org/10.1186/1750-0680-3-7, 2008.

Arya, L. M. and Paris, J. F.: A physicoempirical model to predict the soil moisture characteristic from particle-size distribution and bulk density data, Soil Science Society of America Journal, 45, 1023–1030, https://doi.org/10.2136/sssaj1981.03615995004500060004x, 1981.

Bagley, J. E., Kueppers, L. M., Billesbach, D. P., Williams, I. N., Biraud, S. C., and Torn, M. S.: The influence of land cover on surface energy partitioning and evaporative fraction regimes in the U.S. Southern Great Plains, JGR Atmospheres, 122, 5793–5807, https://doi.org/10.1002/2017JD026740, 2017.

Beck, H. E., Zimmermann, N. E., McVicar, T. R., Vergopolan, N., Berg, A., and Wood, E. F.: Present and future Köppen-Geiger climate classification maps at 1-km resolution, Sci Data, 5, 180214, https://doi.org/10.1038/sdata.2018.214, 2018.

Berryman, E. M., Vanderhoof, M. K., Bradford, J. B., Hawbaker, T. J., Henne, P. D., Burns, S. P., Frank, J. M., Birdsey, R. A., and Ryan, M. G.: Estimating soil respiration in a subalpine landscape using point, terrain, climate, and greenness data, JGR Biogeosciences, 123, 3231–3249, https://doi.org/10.1029/2018JG004613, 2018.

Best, M. J., Abramowitz, G., Johnson, H. R., Pitman, A. J., Balsamo, G., Boone, A., Cuntz, M., Decharme, B., Dirmeyer, P. A., Dong, J., Ek, M., Guo, Z., Haverd, V., van den Hurk, B. J. J., Nearing, G. S., Pak, B., Peters-Lidard, C., Santanello, J. A., Stevens, L., and Vuichard, N.: The Plumbing of Land Surface Models: Benchmarking Model Performance, Journal of Hydrometeorology, 16, 1425–1442, https://doi.org/10.1175/JHM-D-14-0158.1, 2015.

Blyth, E., Gash, J., Lloyd, A., Pryor, M., Weedon, G. P., and Shuttleworth, J.: Evaluating the JULES Land Surface Model Energy Fluxes Using FLUXNET Data, Journal of Hydrometeorology, 11, 509–519, https://doi.org/10.1175/2009JHM1183.1, 2010.

Bonan, G. B.: Forests and Climate Change: Forcings, Feedbacks, and the Climate Benefits of Forests, Science, 320, 1444–1449, https://doi.org/10.1126/science.1155121, 2008.

Bonan, G. B., Levis, S., Kergoat, L., and Oleson, K. W.: Landscapes as patches of plant functional types: An integrating concept for climate and ecosystem models, Global Biogeochem. Cycles, 16, 5-1-5–23, https://doi.org/10.1029/2000GB001360, 2002.

Brooke, J. K., Harlow, R. C., Scott, R. L., Best, M. J., Edwards, J. M., Thelen, J.-C., and Weeks, M.: Evaluating the Met Office Unified Model land surface temperature in Global Atmosphere/Land 3.1 (GA/L3.1), Global Atmosphere/Land 6.1 (GA/L6.1) and limited area 2.2 km configurations, Geosci. Model Dev., 12, 1703–1724, https://doi.org/10.5194/gmd-12-1703-2019, 2019.

Chu, H., Luo, X., Ouyang, Z., Chan, W. S., Dengel, S., Biraud, S. C., Torn, M. S., Metzger, S., Kumar, J., Arain, M. A., Arkebauer, T. J., Baldocchi, D., Bernacchi, C., Billesbach, D., Black, T. A., Blanken, P. D., Bohrer, G., Bracho, R., Brown, S., Brunsell, N. A., Chen, J., Chen, X., Clark, K., Desai, A. R., Duman, T., Durden, D., Fares, S., Forbrich, I., Gamon, J. A., Gough, C. M., Griffis, T., Helbig, M., Hollinger, D., Humphreys, E., Ikawa, H., Iwata, H., Ju, Y., Knowles, J. F., Knox, S. H., Kobayashi, H., Kolb, T., Law, B., Lee, X., Litvak, M., Liu, H., Munger, J. W., Noormets, A., Novick, K., Oberbauer, S. F., Oechel, W., Oikawa, P., Papuga, S. A., Pendall, E., Prajapati, P., Prueger, J., Quinton, W. L., Richardson, A. D., Russell, E. S., Scott, R. L., Starr, G., Staebler, R., Stoy, P. C., Stuart-Haëntjens, E., Sonnentag, O., Sullivan, R. C., Suyker, A., Ueyama, M., Vargas, R., Wood, J. D., and Zona, D.: Representativeness of Eddy-Covariance flux footprints for areas surrounding AmeriFlux sites, Agricultural and Forest Meteorology, 301–302, 108350, https://doi.org/10.1016/j.agrformet.2021.108350, 2021.

Crow, W. T., Kumar, S. V., and Bolten, J. D.: On the utility of land surface models for agricultural drought monitoring, Hydrol. Earth Syst. Sci., 16, 3451–3460, https://doi.org/10.5194/hess-16-3451-2012, 2012.

Dai, Y., Zeng, X., Dickinson, R. E., Baker, I., Bonan, G. B., Bosilovich, M. G., Denning, A. S., Dirmeyer, P. A., Houser, P. R., Niu, G., Oleson, K. W., Schlosser, C. A., and Yang, Z.-L.: The Common Land Model, Bulletin of the American Meteorological Society, 84, 1013–1024, https://doi.org/10.1175/BAMS-84-8-1013, 2003.

520 Dai, Y., Shangguan, W., Wei, N., Xin, Q., Yuan, H., Zhang, S., Liu, S., Lu, X., Wang, D., and Yan, F.: A review of the global soil property maps for Earth system models, SOIL, 5, 137–158, https://doi.org/10.5194/soil-5-137-2019, 2019a.

Dai, Y., Yuan, H., Xin, Q., Wang, D., Shangguan, W., Zhang, S., Liu, S., and Wei, N.: Different representations of canopy structure—A large source of uncertainty in global land surface modeling, Agricultural and Forest Meteorology, 269–270, 119–135, https://doi.org/10.1016/j.agrformet.2019.02.006, 2019b.

525 Dai, Y., Wei, N., Yuan, H., Zhang, S., Shangguan, W., Liu, S., Lu, X., and Xin, Y.: Evaluation of Soil Thermal Conductivity Schemes for Use in Land Surface Modeling, J Adv Model Earth Syst, 11, 3454–3473, https://doi.org/10.1029/2019MS001723, 2019c.

Dirmeyer, P. A.: The terrestrial segment of soil moisture-climate coupling, Geophys. Res. Lett., 38, L16702, https://doi.org/10.1029/2011GL048268, 2011.

530 Dy, C. Y. and Fung, J. C. H.: Updated global soil map for the Weather Research and Forecasting model and soil moisture initialization for the Noah land surface model, JGR Atmospheres, 121, 8777–8800, https://doi.org/10.1002/2015JD024558, 2016.

Entekhabi, D., Rodriguez-Iturbe, I., and Castelli, F.: Mutual interaction of soil moisture state and atmospheric processes, Journal of Hydrology, 184, 3–17, https://doi.org/10.1016/0022-1694(95)02965-6, 1996.

535 Essery, R.: Large-scale simulations of snow albedo masking by forests, Geophysical Research Letters, 40, 5521–5525, https://doi.org/10.1002/grl.51008, 2013.

Forzieri, G., Miralles, D. G., Ciais, P., Alkama, R., Ryu, Y., Duveiller, G., Zhang, K., Robertson, E., Kautz, M., Martens, B., Jiang, C., Arneth, A., Georgievski, G., Li, W., Ceccherini, G., Anthoni, P., Lawrence, P., Wiltshire, A., Pongratz, J., Piao, S., Sitch, S., Goll, D. S., Arora, V. K., Lienert, S., Lombardozzi, D., Kato, E., Nabel, J. E. M. S., Tian, H., Friedlingstein, P., 540 and Cescatti, A.: Increased control of vegetation on global terrestrial energy fluxes, Nat. Clim. Chang., 10, 356–362, https://doi.org/10.1038/s41558-020-0717-0, 2020.

Harper, A. B., Williams, K. E., McGuire, P. C., Duran Rojas, M. C., Hemming, D., Verhoef, A., Huntingford, C., Rowland, L., Marthews, T., Breder Eller, C., Mathison, C., Nobrega, R. L. B., Gedney, N., Vidale, P. L., Otu-Larbi, F., Pandey, D., Garrigues, S., Wright, A., Slevin, D., De Kauwe, M. G., Blyth, E., Ardö, J., Black, A., Bonal, D., Buchmann, N., Burban, B., 545 Fuchs, K., de Grandcourt, A., Mammarella, I., Merbold, L., Montagnani, L., Nouvellon, Y., Restrepo-Coupe, N., and Wohlfahrt, G.: Improvement of modeling plant responses to low soil moisture in JULESvn4.9 and evaluation against flux tower measurements, Geosci. Model Dev., 14, 3269–3294, https://doi.org/10.5194/gmd-14-3269-2021, 2021.

Harper, K. L., Lamarche, C., Hartley, A., Peylin, P., Ottlé, C., Bastrikov, V., San Martín, R., Bohnenstengel, S. I., Kirches, G., Boettcher, M., Shevchuk, R., Brockmann, C., and Defourny, P.: A 29-year time series of annual 300 m resolution plant-550 functional-type maps for climate models, Earth Syst. Sci. Data, 15, 1465–1499, https://doi.org/10.5194/essd-15-1465-2023, 2023.

Humphrey, V., Berg, A., Ciais, P., Gentine, P., Jung, M., Reichstein, M., Seneviratne, S. I., and Frankenberg, C.: Soil moisture–atmosphere feedback dominates land carbon uptake variability, Nature, 592, 65–69, https://doi.org/10.1038/s41586-021-03325-5, 2021.

555 Launiainen, S., Katul, G. G., Kolari, P., Lindroth, A., Lohila, A., Aurela, M., Varlagin, A., Grelle, A., and Vesala, T.: Do the energy fluxes and surface conductance of boreal coniferous forests in Europe scale with leaf area?, Glob Change Biol, 22, 4096–4113, https://doi.org/10.1111/gcb.13497, 2016.

Li, J., Chen, F., Zhang, G., Barlage, M., Gan, Y., Xin, Y., and Wang, C.: Impacts of land cover and soil texture uncertainty on land model simulations over the central Tibetan Plateau, J. Adv. Model. Earth Syst., 10, 2121–2146,
560 https://doi.org/10.1029/2018MS001377, 2018.

Li, J., Zhang, G., Chen, F., Peng, X., and Gan, Y.: Evaluation of land surface subprocesses and their impacts on model performance with global flux data, J. Adv. Model. Earth Syst., 11, 1329–1348, https://doi.org/10.1029/2018MS001606, 2019.

Lin, W., Yuan, H., Dong, W., Zhang, S., Liu, S., Wei, N., Lu, X., Wei, Z., Hu, Y., and Dai, Y.: Reprocessed MODIS Version 6.1 Leaf Area Index Dataset and Its Evaluation for Land Surface and Climate Modeling, Remote Sensing, 15, 1780,
565 https://doi.org/10.3390/rs15071780, 2023.

Mariotti, A., Ruti, P. M., and Rixen, M.: Progress in subseasonal to seasonal prediction through a joint weather and climate community effort, npj Clim Atmos Sci, 1, 4, https://doi.org/10.1038/s41612-018-0014-z, 2018.

Melton, J. R., Arora, V. K., Wisernig-Cojoc, E., Seiler, C., Fortier, M., Chan, E., and Teckentrup, L.: CLASSIC v1.0: the open-source community successor to the Canadian Land Surface Scheme (CLASS) and the Canadian Terrestrial Ecosystem
570 Model (CTEM) – Part 1: Model framework and site-level performance, Geosci. Model Dev., 13, 2825–2850, https://doi.org/10.5194/gmd-13-2825-2020, 2020.

Ménard, C. B., Ikonen, J., Rautiainen, K., Aurela, M., Arslan, A. N., and Pulliainen, J.: Effects of Meteorological and Ancillary Data, Temporal Averaging, and Evaluation Methods on Model Performance and Uncertainty in a Land Surface Model, Journal of Hydrometeorology, 16, 2559–2576, https://doi.org/10.1175/JHM-D-15-0013.1, 2015.

575 Minasny, B. and McBratney, A. B.: Estimating the Water Retention Shape Parameter from Sand and Clay Content, Soil Sci. Soc. Am. J., 71, 1105–1110, https://doi.org/10.2136/sssaj2006.0298N, 2007.

Pastorello, G., Trotta, C., and Canfora, E.: The FLUXNET2015 dataset and the ONEFlux processing pipeline for eddy covariance data, Scientific Data, 7, 225, https://doi.org/10.1038/s41597-021-00851-9, 2020.

Pitman, A. J.: The evolution of, and revolution in, land surface schemes designed for climate models, Int. J. Climatol., 23,
580 479–510, https://doi.org/10.1002/joc.893, 2003.

Poulter, B., Ciais, P., Hodson, E., Lischke, H., Maignan, F., Plummer, S., and Zimmermann, N. E.: Plant functional type mapping for earth system models, Geosci. Model Dev., 4, 993–1010, https://doi.org/10.5194/gmd-4-993-2011, 2011.

Purdy, A. J., Fisher, J. B., Goulden, M. L., and Famiglietti, J. S.: Ground heat flux: An analytical review of 6 models evaluated at 88 sites and globally, J. Geophys. Res. Biogeosci., 121, 3045–3059, https://doi.org/10.1002/2016JG003591,
585 2016.

Shangguan, W., Dai, Y., Duan, Q., Liu, B., and Yuan, H.: A global soil data set for earth system modeling, J. Adv. Model. Earth Syst., 6, 249–263, https://doi.org/10.1002/2013MS000293, 2014.

Shi, J., & Yuan, H., Lin, W., & Dong, W.: A flux tower site attribute dataset intended for land surface modeling [Data set]. Zenodo. https://doi.org/10.5281/zenodo.10939725.

590   Stevens, D., Miranda, P. M. A., Orth, R., Boussetta, S., Balsamo, G., and Dutra, E.: Sensitivity of Surface Fluxes in the ECMWF Land Surface Model to the Remotely Sensed Leaf Area Index and Root Distribution: Evaluation with Tower Flux Data, Atmosphere, 11, 1362, https://doi.org/10.3390/atmos11121362, 2020.

Still, C. J., Berry, J. A., Collatz, G. J., and DeFries, R. S.: Global distribution of C_3 and C_4 vegetation: Carbon cycle implications, Global Biogeochem. Cycles, 17, 6-1-6–14, https://doi.org/10.1029/2001GB001807, 2003.

595   Stockli, R., Lawrence, D. M., Bonan, G. B., Denning, A. S., and Running, S. W.: Use of FLUXNET in the Community Land Model development, J. Geophys. Res., 113, 19, https://doi.org/10.1029/2007JG000562, 2008.

Swenson, S. C., Burns, S. P., and Lawrence, D. M.: The Impact of Biomass Heat Storage on the Canopy Energy Balance and Atmospheric Stability in the Community Land Model, J Adv Model Earth Syst, 11, 83–98, https://doi.org/10.1029/2018MS001476, 2019.

600   Ukkola, A. M., De Kauwe, M. G., Pitman, A. J., Best, M. J., Abramowitz, G., Haverd, V., Decker, M., and Haughton, N.: Land surface models systematically overestimate the intensity, duration and magnitude of seasonal-scale evaporative droughts, Environ. Res. Lett., 11, 104012, https://doi.org/10.1088/1748-9326/11/10/104012, 2016a.

Ukkola, A. M., Pitman, A. J., Decker, M., De Kauwe, M. G., Abramowitz, G., Kala, J., and Wang, Y.-P.: Modelling evapotranspiration during precipitation deficits: identifying critical processes in a land surface model, Hydrol. Earth Syst.
605   Sci., 20, 2403–2419, https://doi.org/10.5194/hess-20-2403-2016, 2016b.

Ukkola, A. M., Haughton, N., De Kauwe, M. G., Abramowitz, G., and Pitman, A. J.: FluxnetLSM R package (v1.0): a community tool for processing FLUXNET data for use in land surface modelling, Geosci. Model Dev., 10, 3379–3390, https://doi.org/10.5194/gmd-10-3379-2017, 2017.

Ukkola, A. M., Abramowitz, G., and De Kauwe, M. G.: A flux tower dataset tailored for land model evaluation, Earth Syst.
610   Sci. Data, 14, 449–461, https://doi.org/10.5194/essd-14-449-2022, 2022.

Williams, I. N. and Torn, M. S.: Vegetation controls on surface heat flux partitioning, and land-atmosphere coupling, Geophysical Research Letters, 42, 9416–9424, https://doi.org/10.1002/2015GL066305, 2015.

Williams, M., Richardson, A. D., Reichstein, M., Stoy, P. C., Peylin, P., Verbeeck, H., Carvalhais, N., Jung, M., Hollinger, D. Y., Kattge, J., Leuning, R., Luo, Y., Tomelleri, E., and Trudinger, C. M.: Improving land surface models with FLUXNET
615   data, Biogeosciences, 6, 1341–1359, https://doi.org/10.5194/bg-6-1341-2009, 2009.

Wilson, K., Goldstein, A., Falge, E., Aubinet, M., Baldocchi, D., Berbigier, P., Bernhofer, C., Ceulemans, R., Dolman, H., Field, C., Grelle, A., Ibrom, A., Law, B. E., Kowalski, A., Meyers, T., Moncrieff, J., Monson, R., Oechel, W., Tenhunen, J., Valentini, R., and Verma, S.: Energy balance closure at FLUXNET sites, Agricultural and Forest Meteorology, 113, 223–243, https://doi.org/10.1016/S0168-1923(02)00109-0, 2002.

620   Zhang, X., Dai, Y., Cui, H., Dickinson, R. E., Zhu, S., Wei, N., Yan, B., Yuan, H., Shangguan, W., Wang, L., and Fu, W.: Evaluating common land model energy fluxes using FLUXNET data, Adv. Atmos. Sci., 34, 1035–1046, https://doi.org/10.1007/s00376-017-6251-y, 2017.

Zhu, S., Chen, H., Zhang, X., Wei, N., Shangguan, W., Yuan, H., Zhang, S., Wang, L., Zhou, L., and Dai, Y.: Incorporating root hydraulic redistribution and compensatory water uptake in the Common Land Model: Effects on site level and global
625   land modeling, J. Geophys. Res. Atmos., 122, 7308–7322, https://doi.org/10.1002/2016JD025744, 2017.